Acta Mech Sin (2009) 25:303–310
DOI 10.1007/s10409-009-0242-x

RESEARCH PAPER

Multi-scale calculation of settling speed of coarse particles by accelerated Stokesian dynamics without adjustable parameter

Long Wang · Jiachun Li · Jifu Zhou

Received: 13 November 2008 / Accepted: 4 January 2009 / Published online: 8 April 2009

Abstract The calculation of settling speed of coarse particles is firstly addressed, with accelerated Stokesian dynamics without adjustable parameters, in which far field force acting on the particle instead of particle velocity is chosen as dependent variables to consider inter-particle hydrodynamic interactions. The sedimentation of a simple cubic array of spherical particles is simulated and compared to the results available to verify and validate the numerical code and computational scheme. The improved method keeps the same computational cost of the order $O(N \log N)$ as usual accelerated Stokesian dynamics does. Then, more realistic random suspension sedimentation is investigated with the help of Mont Carlo method. The computational results agree well with experimental fitting. Finally, the sedimentation of finer cohesive particle, which is often observed in estuary environment, is presented as a further application in coastal engineering.

Keywords Sedimentation · Stokesian dynamics · Many-body interactions · Multi-scale

1 Introduction

Particle suspension dispersion systems play important roles in coastal engineering, in which particle settling speed is a crucial factor in parameterizations to simulate sediment transport [1]. The sedimentation of particles in the real environment is rather complex. In the river, particles may move in group, the behavior of which is totally different from that of a single particle. And in estuary, the charge on the fine silt particles would cause the formation of flocs, whose settling speed is a few orders of magnitude larger than that of discrete particles. Many factors such as particle size distribution, salinity, turbulence, etc. have effects on sedimentation. However, the most fundamental consideration among them is inter-particle hydrodynamic interaction for particle with radius ranging from microns to a few millimeters. With emphasis on the hydrodynamic force in this paper, the attention is mainly paid to the sedimentation of coarse particles in still water. For coarse particles, gravity is the only external force while Brownian motion and physicochemical interaction are neglected.

As we know, classical Stokes formula

$$U_0 = \frac{2}{9}\frac{a^2(\rho_p - \rho_w)}{\mu}g, \tag{1}$$

gives settling speed for a single sphere in unbounded domain. For multi-particle system, the falling speed can be directly expressed as

$$U = U_0 f(\phi),$$

where $f(\phi)$ is hindered settling function, ϕ volume fraction. U_0 denotes Stokesian settling speed for a single particle. Great efforts have been made to study the form of $f(\phi)$. Richardson and Zaki gave an empirical formula

$$f(\phi) = (1-\phi)^n, \tag{2}$$

where n is an empirical constant. Some other theoretical or empirical formula are summarized by Tory [2] as follows. A semi-empirical formula

The project supported by the National Natural Science Foundation of China (10332050 and 10572144) and Knowledge Innovation Program (KJCX-SW-L08).

L. Wang · J. Li (✉) · J. Zhou
Institute of Mechanics, CAS, 100190 Beijing, China
e-mail: jcli05@imech.ac.cn

$$f(\phi) = \frac{(1-\phi)^2}{(1+\phi^{1/3})\exp(5\phi/3(1-\phi))} \tag{3}$$

was put forward by Barnea and Mizrahi. Cell model was applied by Happel to give a theoretical formula

$$f(\phi) = \frac{2-3\phi^{1/3}+3\phi^{5/3}-2\phi^2}{2+4\phi^{5/3}/3}. \tag{4}$$

Besides the application of hydrodynamics for sedimentation, Mills and Snabre [3] determined the function using mean-field approach

$$f(\phi) = \frac{1-\phi}{1+k\phi/(1-\phi)^3}. \tag{5}$$

Although the above formulas are available, the assumption of discrete particles and spatially homogeneous distribution restricts their applications. The sedimentation of particle aggregation, such as flocs in the estuary, can not be estimated by these formulas, since potential interactions between particles or particle shape cannot be taken into consideration by these formula. That is to say, the extrapolation of these formulas to more complicated cases is physically infeasible.

The primary difficulty in modeling particle suspension lies in the large separation of scales. The scale of flow can be up to the order of meters, whereas the interactions between particles take place on the micron scale. It is almost impossible for traditional approaches to cover all length and time scales. Consequently, we have to resort to the multi-scale modeling strategy, namely, the motions of fluid phase and particle phase are simulated on different scale [4]. For particle suspension system, the bulk properties can be obtained by ensemble average of the particle properties. For instance, the settling speed of coarse particles is actually the mean value of settling speed of each individual particle. Thus, large-scale macroscopic properties are collective behavior of small-scale microscopic properties from the multi-scale point of view.

Vincent [5] simulated the sedimentation of a pair of non-spherical particles with boundary element method. Sherwood [6] investigated the motions of the 2-dimensional plate-like particle with Brownian dynamics. However, in the framework of Brownian dynamics, the hydrodynamic interaction is ignored or replaced by addition of two-body interactions. Glendinning and Russel [7] studied sedimentation and diffusion with a pairwise addition. Error sedimentation speed and negative self-diffusion coefficient might probably occur with two-body superposition. Feng and Joseph [8] studied the unsteady motion of particle with finite element method. Lattice Boltzmann method (LBM) is applied by Nguyen et al. [9] to investigate the particle suspension. Boek et al. [10] adopted dissipative particle dynamics(DPD) to research colloidal suspension. In this kind of methods, the motion of fluid phase is simulated on the mesoscopic level, which means more computational cost is required on calculation of fluid phase.

On the basis of the superposition of fundamental solution of Stokesian equation for small Reynolds motion, Brady and Bossis [11] developed a method that accounts for both the many-body interactions and the near-field lubrication effects by splitting the hydrodynamic interaction into a far-field mobility and a pairwise additive resistance calculation. The method known as Stokesian dynamics (SD) has been widely used for particle dispersion systems to study hydrodynamic transport properties, rheology and particle microstructure. The main disadvantage of the method SD, however, is that it requires inversion of a far-field mobility matrix with a computational cost of order $O(N^3)$, which limits particle number to only the order of one hundred. For most particle systems, hundreds of particles are needed to capture the microstructure correctly. To avoid both the costly construction of the far-field mobility matrix and its inversion, Sierou and Brady [12] put forward accelerated Stokesian dynamics (ASD), which reduces the computational cost to the order $O(N \log N)$ with the same accuracy as SD by using iterative methods and the particle-mesh-Ewald technique. However, extra parameter is needed to assure the positive definiteness of resulting equation in the method similar to Sierou's.

In order to avoid the extra adjustable parameter, the far-field forces instead of particle velocity are chosen as dependent variables in the present article [13]. Simple-cubic array of spheres sedimentation is firstly calculated and the results are compared with exact solutions. Scaling of the computational cost of this method with particle number is subsequently presented. Then, more realistic random sedimentation is studied by the improved accelerated Stokesian dynamics in excellent agreement with previous formula. Finally, the sedimentation of finer cohesive particles often observed in estuary is examined as an application in coastal engineering.

2 Accelerated Stokesian dynamics without adjustable parameter

The small particle motions can be described with Stokesian equation due to small Reynolds number [14]. The linearity of Stokesian equation relates the particle velocity to the force acting on the particle with mobility matrix:

$$\boldsymbol{M} \cdot \boldsymbol{F} = \boldsymbol{U}, \tag{6}$$

where $\boldsymbol{U}$ is the translational-angular velocities, $\boldsymbol{F}$ is the force-torque vector. In contrast, the inversion problem is then to relate the force to the particle velocity:

$$\boldsymbol{R} \cdot \boldsymbol{U} = \boldsymbol{F}, \tag{7}$$

where $\boldsymbol{R}$ is the resistance matrix.

Very probably, a great many particles involved in real environment, for instance, particles in coastal engineering, is of the characteristics of movement in group, the behavior of which is totally different from the motion of a single particle. The issue in group motion belongs to many-body interactions among particles or the many-body hydrodynamic interactions. Durlofsky et al. [15] developed a method that accounts for both the many-body interactions and the near-field lubrication effects by splitting the hydrodynamic interaction into a far-field mobility $\boldsymbol{M}$ and a pairwise additive resistance calculation. The main disadvantage of the method, however, is that it requires inversion of a far-field mobility matrix with a computational cost of $O(N^3)$ (N is the number of particles in the system), which limits the method to particle number to the order of one hundred. To avoid both the costly construction of the far-field mobility matrix and its inversion, Sierou et al. [12] put forward accelerated Stokesian dynamics (ASD), which reduces the computational cost to the order $O(N \ln N)$ with the same accuracy by using iterative method and particle-mesh-Ewald technique.

The disturbance velocity field at $\boldsymbol{r}$ due to particle m can be written as

$$\boldsymbol{u}(\boldsymbol{r}) = \frac{1}{8\pi\mu}\left(1 + \frac{a^2}{6}\nabla^2\right)\boldsymbol{J}(\boldsymbol{r} - \boldsymbol{r}_m)\cdot\boldsymbol{F}_m + \cdots, \tag{8}$$

where μ is viscosity, a is particle radius, $\boldsymbol{F}_m$ is the force exerted by particle m on fluid, and $\boldsymbol{J}(\boldsymbol{r})$ is Stokeslet or Oseen tensor

$$J_{ij}(\boldsymbol{r}) = \frac{1}{r}\left(\delta_{ij} + \frac{r_i r_j}{r^2}\right).$$

When the fluid velocity is determined by Eq. (8), we can obtain the force exerted by particle n on the fluid by use of Faxen formulas [14] for spheres

$$\boldsymbol{F}_n = 6\pi\mu a\left[\boldsymbol{U}_n - \left(1 + \frac{a^2}{6}\nabla^2\right)\boldsymbol{u}'_n\right], \tag{9}$$

where $\boldsymbol{u}'_n$ is far-field fluid velocity evaluated at the center of the particle n. In the same manner, the force $\boldsymbol{F}_n$ will induce a new force $\boldsymbol{F}_m$. The procedures repeat infinitely until the forces pertinent to the two particles are kept unchanged. This is the essence of reflection method.

The method of reflections of the force version can be expressed in a matrix form as follows [16]

$$\boldsymbol{F}^{(i)} = \boldsymbol{I}_{\mathrm{B}}\cdot\left[\boldsymbol{U} - \tilde{\boldsymbol{M}}\cdot\boldsymbol{F}^{(i-1)}\right], \tag{10}$$

where

$$\boldsymbol{I}_{\mathrm{B}} = -6\pi\mu a\boldsymbol{I},$$

$$(\tilde{\boldsymbol{M}})_{mn} = (1-\delta_{mn})\frac{1}{8\pi\mu}\left(1 + \frac{a^2}{6}\nabla^2\right)^2\boldsymbol{J}(\boldsymbol{r}_m - \boldsymbol{r}_n).$$

The vectors $\boldsymbol{U} = [\boldsymbol{U}_1, \ldots, \boldsymbol{U}_N]^{\mathrm{T}}$, $\boldsymbol{F}^{(i)} = [\boldsymbol{F}_1^{(i)}, \ldots, \boldsymbol{F}_N^{(i)}]^{\mathrm{T}}$ represent the set of particle velocity and force vectors, respectively. $\boldsymbol{I}$ is unit tensor. Ichiki and Brady [16] have shown the equivalence between the method of reflections and inversion of mobility matrix.

Equation (10) is the iteration matrix form of reflection method, and its equivalent direct matrix form turns out

$$(\boldsymbol{I} + \boldsymbol{M}_{\mathrm{ref}})\cdot\boldsymbol{F} = \boldsymbol{I}_{\mathrm{B}}\cdot\boldsymbol{U}, \tag{11}$$

where $\boldsymbol{M}_{\mathrm{ref}} = \boldsymbol{I}_{\mathrm{B}}\cdot\tilde{\boldsymbol{M}}$ is the reflection matrix. One can recognize Eq. (10) as Jacobin iterative method at a glance. When comparing Eq. (6) with Eq. (11), we can understand that the method of reflection is one of many possible iterative methods to obtain the inverse of the mobility matrix and the inverse of the mobility matrix certainly includes many-body interactions.

In near field, a lubrication force in term of matrix $\boldsymbol{R}_{\mathrm{lub}}$ must be introduced when two particles is close to each other due to ignorance of higher order singularities. Thus, in the absence of particle inertia, the particles motion equation can be expressed as

$$\left[\boldsymbol{R}_{\mathrm{lub}} + (\boldsymbol{I} + \boldsymbol{M}_{\mathrm{ref}})^{-1}\cdot\boldsymbol{I}_{\mathrm{B}}\right]\cdot\boldsymbol{U} = -\boldsymbol{F}^{\mathrm{e}}, \tag{12}$$

where $\boldsymbol{F}^{\mathrm{e}}$ is external non-hydrodynamic force exerted on the particles, such as gravity or potential force.

There is an inversion operation in Eq. (12). However, it is inefficient for large system to solve the equation directly. A scheme applied to the resolution of equation can be expressed as

$$-\boldsymbol{R}_{\mathrm{lub}}\cdot\boldsymbol{U} = \boldsymbol{F}^{\mathrm{e}} + \boldsymbol{F}_{\mathrm{ff}}, \tag{13}$$

where

$$\boldsymbol{F}_{\mathrm{ff}} = (\boldsymbol{I} + \boldsymbol{M}_{\mathrm{ref}})^{-1}\cdot\boldsymbol{I}_{\mathrm{B}}\cdot\boldsymbol{U} \tag{14}$$

indicates the far-field hydrodynamic force which is solved in advance. In order to guarantee the positive definiteness of the lubrication matrix $\boldsymbol{R}_{\mathrm{lub}}$, however, an extra parameter β is needed to add to both sides of Eq. (13). The final particle motion equation looks like

$$-(\boldsymbol{R}_{\mathrm{lub}} + \beta\boldsymbol{I})\cdot\boldsymbol{U}^{\mathrm{new}} = \boldsymbol{F}^{\mathrm{e}} + \boldsymbol{F}_{\mathrm{ff}} - \beta\boldsymbol{I}\cdot\boldsymbol{U}^{\mathrm{old}}, \tag{15}$$

which is identical to that used in Sierou method [12] if $\beta = 1$.

There are some drawbacks in this scheme. First of all, to achieve satisfying convergent rate, the parameter β should be carefully chosen. Many tests are required under different conditions. Secondly, we may always find disagreement between the velocity $\boldsymbol{U}^{\mathrm{new}}$ and $\boldsymbol{U}^{\mathrm{old}}$. In order to keep their consistency, an additional iterative scheme is needed. And finally, the far-field force $\boldsymbol{F}_{\mathrm{ff}}$ is actually calculated based on the velocity $\boldsymbol{U}^{\mathrm{old}}$ instead of $\boldsymbol{U}^{\mathrm{new}}$.

The unknowns associated with a particle are velocity $\boldsymbol{U}$ and hydrodynamic force $\boldsymbol{F}$. The above method chooses the

velocity $\boldsymbol{U}$ as unknowns. As an alternative, hydrodynamic force $\boldsymbol{F}$ can be chosen as unknowns, thus resulting in a mathematically consistent scheme. In particular, the scheme facilitates to avoid an extra parameter and additional iterations.

As a result, Eq. (13) can be rewritten as

$$\boldsymbol{R}_{\text{lub}} \cdot \boldsymbol{U} + \boldsymbol{F}_{\text{ff}} = -\boldsymbol{F}^{\text{e}}. \tag{16}$$

With the aid of Eq. (14), the velocity $\boldsymbol{U}$ in Eq. (16) is replaced by hydrodynamic force $\boldsymbol{F}_{\text{ff}}$. So, the equation with force as dependent variables can be expressed as

$$\boldsymbol{R}_{\text{lub}} \cdot \boldsymbol{I}_{\text{B}}^{-1} \cdot (\boldsymbol{I} + \boldsymbol{M}_{\text{ref}}) \cdot \boldsymbol{F}_{\text{ff}} + \boldsymbol{F}_{\text{ff}} = -\boldsymbol{F}^{\text{e}}. \tag{17}$$

Once the far-field force is calculated, the Faxen formula is again used to obtain the particle velocity.

In the present scheme, the left side of Eq. (17) includes both far-field and near-field force. In contrast, the previous mentioned particle motion Eq. (15) only involves near field lubrication force at the left side. Such a difference leads to the necessity of an extra parameter. The further reason comes from Eq. (12). In order to avoid the inversion operation at the left side of Eq. (12), the far-field force should be given in advance. So, the far-field and near-field forces can not be solved simultaneously. If force is chosen as dependent variables, the involved inversion operation disappears, which permits the solution of both far-field and near-field force concurrently, just as stated in Eq. (17).

To speed up the calculation of Eq. (17), a conjugate gradient-type iterative method, GMRES (generalized minimum residual) method is applied. The crucial step in GMRES is to implement the matrix-vector multiplication of the reflection matrix $\boldsymbol{M}_{\text{ref}}$ with far-field force $\boldsymbol{F}_{\text{ff}}$. For this purpose, particle mesh Ewald technique is used, which is described in detailed by Sierou and Brady [12].

3 Validation of the method

To validate the method, the sedimentation of a simple cubic array of sphere is calculated. The initial position of spheres is given by

$$\boldsymbol{r}_n = n_1\boldsymbol{a}^1 + n_2\boldsymbol{a}^2 + n_3\boldsymbol{a}^3, \quad n_1, n_2, n_3 = 0, \pm1, \pm2, \ldots,$$

where $\boldsymbol{a}^i$, $i = 1, 2, 3$ is base vector between two spheres. For simple cubic array,

$$\begin{bmatrix} \boldsymbol{a}^1 \\ \boldsymbol{a}^2 \\ \boldsymbol{a}^3 \end{bmatrix} = h \begin{bmatrix} 1 & 0 & 0 \\ 0 & 1 & 0 \\ 0 & 0 & 1 \end{bmatrix},$$

h is a parameter representing the distance between spheres.

Hasimoto [17] has provided an asymptotic approximation for dilute concentration. For simple cubic array, the relationship between settling speed and concentration is

$$U_s/U_0 = 1 - 1.7601\phi^{1/3} + \phi - 1.5593\phi^2 + \cdots. \tag{18}$$

Sangani and Acrivos [18] started from the Hasimoto fundamental solution and gave a more accurate formula

$$U_s/U_0 = 1 - 1.7601\phi^{1/3} + \phi - 1.5593\phi^2 + 3.9799\phi^{8/3} - 3.0734\phi^{10/3} + \cdots. \tag{19}$$

Zick and Homsy [19] obtained numeric solution from Fredholm integral equations of the first kind.

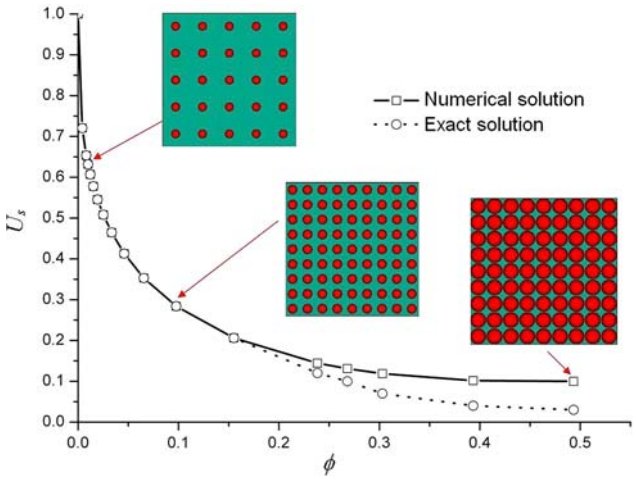

Fig. 1 The dimensionless sedimentation speed U_s of SC array of spheres with different volume concentration (%). Good agreement between these results is presented when volume concentration is less than 20%

The settling speed U_s is non-dimensionalized in terms of U_0 in Fig. 1. We may find that the results are almost identical to the exact solution as the volume fraction is less than 20% and they tend to overestimate the sedimentation speed for larger volume fraction. The reason for the fact is attributed to the omission of high-order multipoles.

4 Computation scheme and results

In order to accelerate matrix-vector multiplication of the reflection matrix $\boldsymbol{M}_{\text{ref}}$ with far-field force $\boldsymbol{F}_{\text{ff}}$, particle-mesh Ewald method is used. The method starts from Hasimoto's fundamental solution [17] and splits the far-field force into real-part sum and wave-part sum by applying of splitting factor α. The velocity field introduced by wave-part sum is

$$u_i^{WS}(\boldsymbol{r}) = \sum_{k\neq0} \frac{2\pi\alpha}{V_0} \left\{k^2\delta_{ij} - k_i k_j\right\} \phi_1(\pi\alpha k^2) \times \left(\sum_p \frac{F_j(\boldsymbol{r}_p)}{8\pi\mu} \mathrm{e}^{2\pi \mathrm{i}\boldsymbol{k}\cdot\boldsymbol{r}_p}\right) \mathrm{e}^{-2\pi\mathrm{i}\boldsymbol{k}\cdot\boldsymbol{r}}, \tag{20}$$

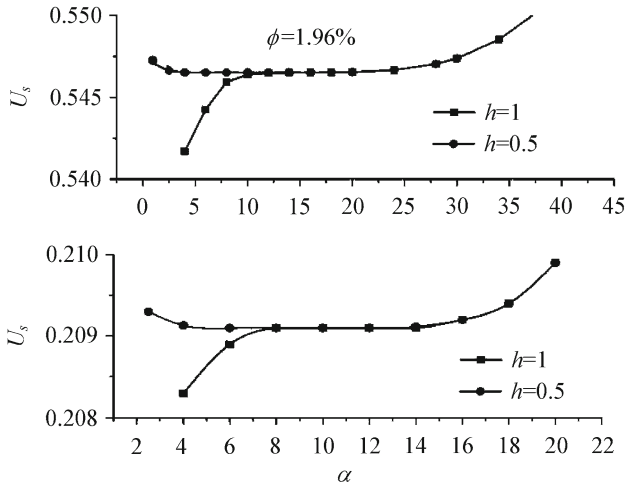

Fig. 2 The effect of splitting factor α on dimensionless settling speed. The refinement of grid extends the plateau to smaller α region where wave-part sum is dominant. The real-part sum is independent of grid size for larger α

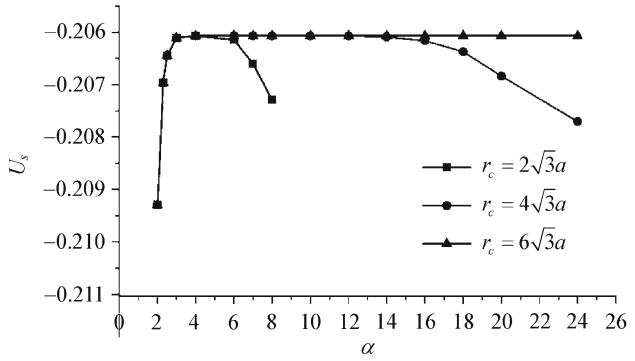

Fig. 3 The effect of cutoff radius r_c on dimensionless settling speed. With the increment of cutoff radius, the plateau extends to larger α and has no effect on small α

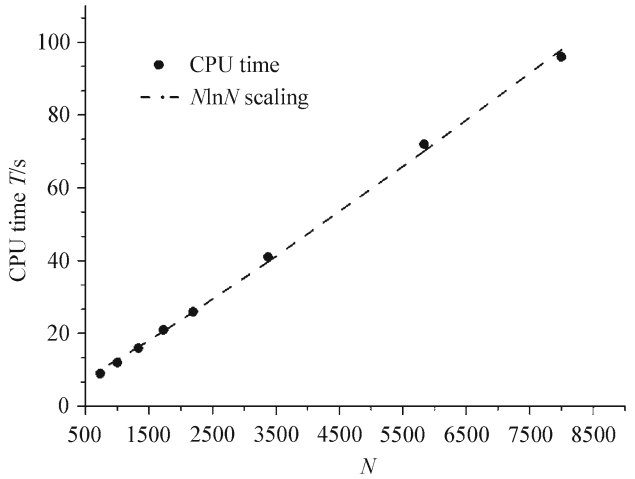

Fig. 4 The CPU time T as function of particle number N. With the increment of particle number, the CPU time increases according to the scale of $N \log N$

where V_0 is the volume of the computational domain, k is wave number, ϕ_ν is incomplete Γ-function. For wave-part sum, the force acting on the particle is distributed on the mesh and fast Fourier transform is used to keep the computational cost to the order $O(N \log N)$. The velocity field introduced by real-part sum is

$$u_i^{RS}(\boldsymbol{r}) = \frac{1}{4\pi\mu}\sum_n F_j^n\Big[-\frac{\pi}{\alpha^{3/2}}\bar{r}^2\phi_{1/2}\delta_{ij} + \alpha^{-1/2}\phi_{-1/2}\delta_{ij} + \frac{\pi}{\alpha^{3/2}}\bar{r}_i\bar{r}_j\phi_{1/2}\Big], \tag{21}$$

where $\bar{\boldsymbol{r}} = \boldsymbol{r} - \boldsymbol{r}_n$. For real-part sum only particles within the cutoff radius r_c of a particle are considered in order to reduce the computational cost to the order of $O(N)$. Therefore, the overall computational cost is of the order $O(N \log N)$.

The effect of splitting factor α on settling speed is displayed for $\phi = 1.96$ and 15.5% in Fig. 2. The wave-part sum becomes dominant for smaller α while the real-part sum is more important for larger α. Since a plateau can be observed in Fig. 2, the splitting factor α is suggested to be chosen in the range where settling speed is insensitive to α. For refined mesh, the plateau can be extended leftward to smaller α. Since real-part sum is independent of mesh size, the refinement of mesh exhibits no effect for larger α.

The effect of cutoff radius r_c on settling speed is shown in Fig. 3. With the increment of cutoff radius from $2\sqrt{3}a$ to $4\sqrt{3}a$, $6\sqrt{3}a$, the plateau extends to large α, and exhibits no effect on small α. The choice of splitting factor, cutoff radius and mesh size are critical for the acceleration of computation.

The efficiency of the method is displayed in Fig. 4 where CPU time (in seconds) versus the particle number N is plotted. The configurations of the particles in this case are regular simple-cubic array. The volume fraction of particles is 45.2%. Figure 4 shows that the actual calculation time accords with the expected $N \ln N$ scaling law. In order to speed up the calculation, parallel technique with OpenMP is adopted. Figure 5 presents the accelerate ratio, which exhibits good linearity with CPU number.

On the basis of the above description, coarse particle sedimentation of more realistic random suspension is calculated by using Mont Carlo approach. The positions of particles are randomly generated and then checked whether the location has been previously occupied by other particles. If true, a new position is regenerated again until all the positions of particles are specified as an initial state. Then the simulation of particle sedimentation is started. The procedure stops when a stable statistical average sedimentation speed is reached. The gravity is the only external force and 1,000 particles are used in the calculations. As Phillips [20] and Ladd [21] pointed out, the sedimentation system size may exert apparent effects on settling speed as observed in Figs. 6 and 7.

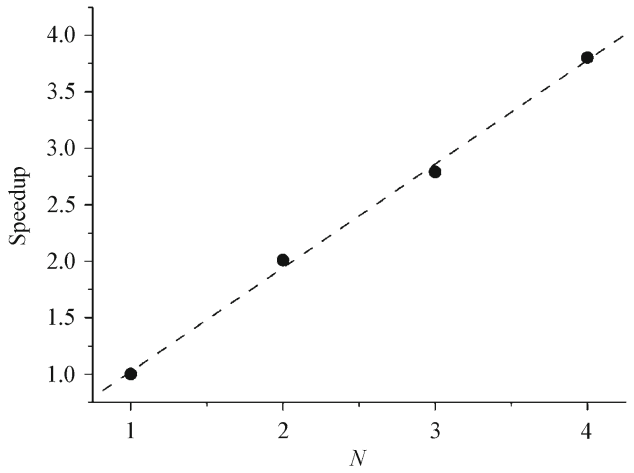

Fig. 5 The parallel performance: accelerate ratio with OpenMP. The good linear relation between CPU number N and speedup is shown

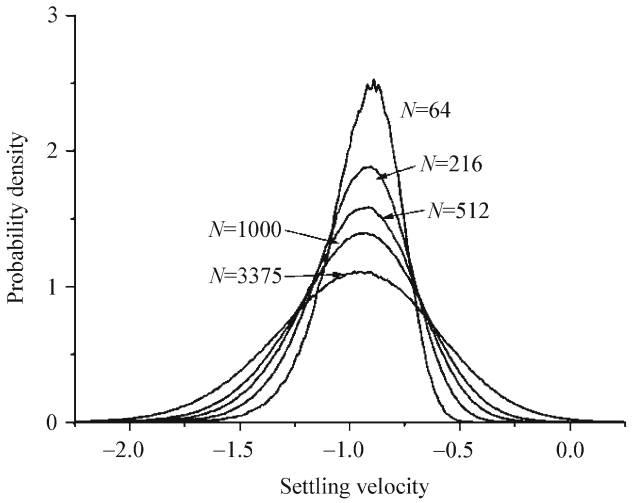

Fig. 6 Probability density functions of non-dimensional sedimentation speed with different particle number N in the case of volume fraction 0.124%

Figure 6 shows the PDF (probability density function) of sedimentation speed with different particle number N for volume fraction 0.124%. With the growth of particle number, the shape of PDF becomes more flatter, which implies the randomness in the system is enhanced.

The effect of system size on sedimentation speed can be estimated by the formula [20]

$$\Delta U \sim (\phi/N)^{1/3}. \tag{22}$$

It means that the deviation from the mean settling speed drops while we use many more particles. Mo and Sangani [22] gave a corrected sedimentation speed formula

$$U_s = U_s(N) + 1.7601(\phi/N)^{1/3}\mu_r S(0)U_0, \tag{23}$$

where

$$\mu_r = 1 + 2.5\phi + 7.35\phi^2, \tag{24}$$

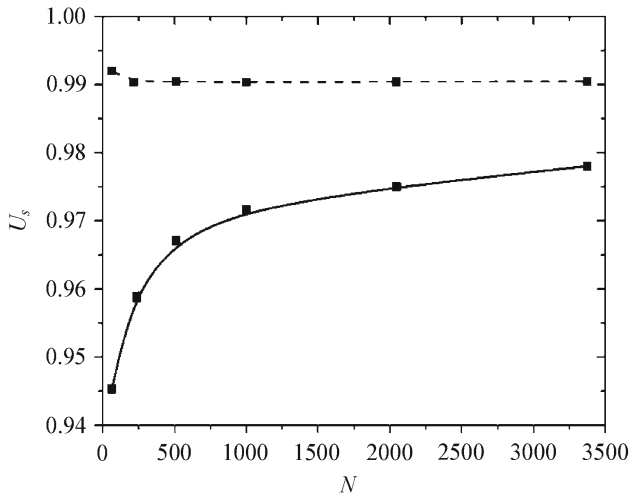

Fig. 7 The non-dimensional sedimentation speed as function of particle number in the case of volume fraction of 0.124%. The *solid line* is computational results. The *dashed line* is corrected sedimentation speed, which is independent of particle number

$$S(0) = \frac{(1-\phi)^4}{1 + 4\phi + 4\phi^2 - 4\phi^3 + \phi^4}. \tag{25}$$

In Eq. (23), $U_s(N)$ is the variation of computational results with particle number N. On the other hand, Fig. 7 shows the corrected sedimentation speed for volume fraction of different particle number. The corrected sedimentation speed are nearly constant, independent of particle number, which proves the validity of the presented calculation results.

The effects of volume fraction on sedimentation speed are displayed in Fig. 8. There are 1,000 particles used for all runs, and results are corrected by Eq. (23). Richardson and Zaki formula is fitted with $n = 5.9$ in the present study. In Fig. 8, we may see that corrected results and fitting data by Eq. (23), denoted by solid circle and triangle, respectively, are very close. Very probably the small deviation is partially due to the truncation of multipole expansion and partially due to the non-uniform particle size in experiments.

5 Further application in the cohesive particles suspension system

The sediment grains in the estuary usually are finer cohesive particles. Due to physicochemical property, cohesive particles commonly aggregate into flocs. The conventional explanation of flocculation is based on DLVO theory. Namely, van der Waals attraction and double layer repulsion constitutes DLVO theory framework. The counter-ions in the water are attracted by charge on the particle surface and give rise to double electric layer. For constant charge density, the electrostatic energy V_r can be expressed as:

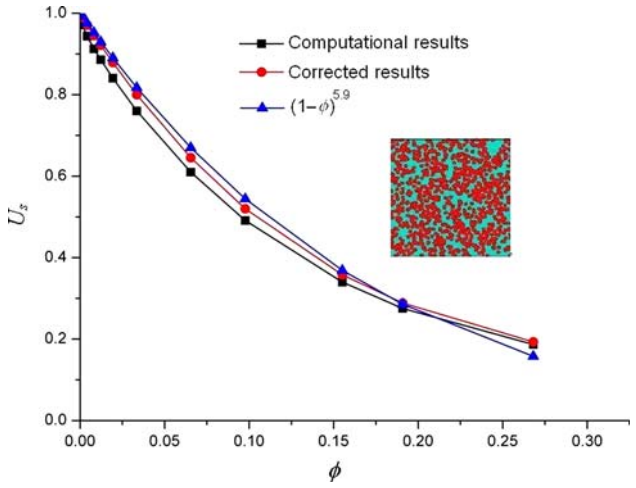

Fig. 8 The dimensionless random sedimentation speed dependence on volume fraction. The *solid square* is computational results, the *solid circle* is corrected results, and the *solid triangle* is fitting data with RZ formula

$$V_r = -2\pi a\varepsilon\psi^2 \ln\left(1 - \mathrm{e}^{-\kappa h}\right), \tag{26}$$

where ε is the dielectric constant of water, a is particle radius, ψ is surface potential, κ^{-1} is the Debye reciprocal length and h is the closest distance between two particles. The van der Waals attractive energy V_a can be expressed as

$$V_a = -\frac{aA}{12h} f(p), \tag{27}$$

where A is the Hamaker constant and $f(p)$ is the retardation factor, given by the following formula

$$f(p) = \begin{cases} \dfrac{1}{1+1.77p}, & p < 1, \\ \dfrac{2.45}{5p} - \dfrac{2.17}{15p^2} + \dfrac{0.59}{35p^3}, & p > 1, \end{cases} \tag{28}$$

where $p = 2\pi h/\lambda$, λ is London wavelength and usually is 0.1μm. Thus, the overall potential is

$$V_t = V_a + V_r.$$

The effect of electrolyte concentration on flocculation is embodied by the change of Debye reciprocal length κ^{-1}, which can be written as

$$\kappa^{-1} = \sqrt{\frac{\varepsilon k_{\mathrm{B}} T}{2IeF}},$$

where k_{B} is the Boltzmann constant, F is the Faraday constant, T is temperature, e is elementary charge, $I = \frac{1}{2}\sum c_i z_i^2$ is ionic strength (z_i is ionic valence, c_i is ionic molarity). When the electrolyte concentration increases or ionic valence is high, the Debye reciprocal length decreases and the double electric layer gets thinner, which is favorable for particle aggregation.

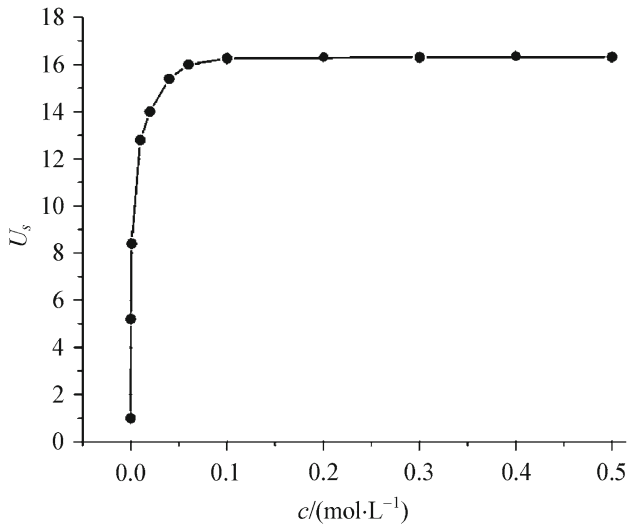

Fig. 9 Dependence of dimensionless settling speed on electrolyte concentration. The abscissa is electrolyte concentration (mol/L), the ordinate is non-dimensional settling speed

Beside hydrodynamic interactions and gravity, DLVO potential between particles is also included in our calculation. The following potential parameters are used in the present study: $A = 4 \times 10^{-20}$ J, $\psi = -250$ mV, $T = 300$ K, $a = 2$ μm, the particle density is 2,650 kg/m^3, the particle weight concentration is 6.424 kg/m^3.

Figure 9 displays the effect of the electrolyte concentration on settling speed. With the increasing of electrolyte concentration, the settling speed rises rapidly until the electrolyte concentration exceeds 0.1 mol/L. The ultimate settling speed almost remains unchanged when the critical value of 0.1 mol/L is reached.

Obviously, the settling speed of flocs is faster than that of coarse particle because they aggregate into flocs (see Fig. 10). This is an indirect result reflecting the effect of salinity on sedimentation. Further study should take such factors as Hamaker constant, surface potential, etc. into consideration in more detail.

6 Conclusions

In this study, the settling speed of coarse particles is investigated with modified accelerated Stokesian dynamics, which avoids the necessity of extra adjustable parameter. The sedimentation simulation of a simple cubic array of spheres as a test is used to validate the method by examining dependence of settling speed on volume fraction. The comparisons with exact solution are satisfying for small volume concentration. The computational cost has been proved to remain the order of $O(N \log N)$. Mont Carlo approach is used to study more realistic random suspension sedimentation. The results agree

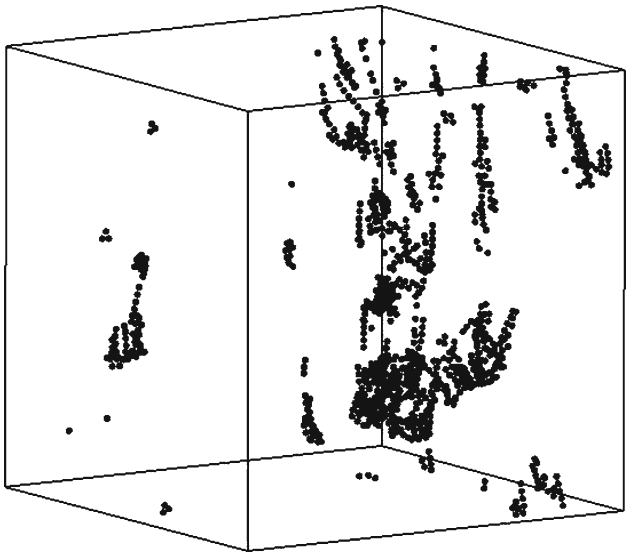

Fig. 10 The aggregation of particles due to potential interactions

well with previous formula. We further apply the method to the sedimentation of fine cohesive particles indicating that the settling speed of flocs is considerably larger than that of coarse particles. The method used in the present paper is capable of predicting the sedimentation behaviors of particle suspension dispersion system in more complicated natural and industrial environments.

References

1. Li, J.C., Zhou, J.F.: Sediment transport mechanism in estuaries and its application. In: Proceeding of 11th Asian Congress of Fluid Mech, pp. 85–95. Kuala Lumpur, Malaysia (2006)
2. Tory, E.M.: Sedimentation of Small Particles in a Viscous Fluid. Computational Mechanics Publications, Southampton (1996)
3. Mills, P., Snabre, P.: Settling of a suspension of hard spheres. Europhys. Lett. **25**, 651–656 (1994)
4. van derHoef, M.A., vanSint Annaland, M., Deen, N.G., Kuipers, J.A.M.: Numerical simulation of dense gas-solid fluidized beds: a multiscale modeling strategy. Annu. Rev. Fluid Mech. **40**, 47–70 (2008)
5. Vincent, J., Phan-Thien, N., Tran-Cong, T.: Sedimentation of multiple particles of arbitrary shape. J. Rheol. **35**, 1–27 (1991)
6. Sherwood, J.D.: Brownian dynamics simulations of a 2-D suspension of charged colloidal plates under shear. J. Non-Newtonian Fluid Mech. **43**, 195–228 (1992)
7. Glendinning, A.B., Russel, W.B.: A pairwise additive description of sedimentation and diffusion in concentrated suspensions of hard spheres. J. Colloid Interface Sci. **89**, 124–143 (1982)
8. Feng, J., Joseph, D.D.: The unsteady motion of solid bodies in creeping flows. J. Fluid Mech. **303**, 83–102 (1995)
9. Nguyen, N.Q., Ladd, A.J.C.: Sedimentation of hard-sphere suspensions at low Reynolds number. J. Fluid Mech. **525**, 73–104 (2005)
10. Boek, E.S., Coveney, P.V., Lekkerkerker, H.N.W., van der Schoot, P.: Simulating the rheology of dense colloidal suspensions using dissipative particle dynamics. Phys. Rev. E **55**, 3124–3133 (1997)
11. Brady, J.F., Bossis, G.: Stokesian dynamics. Ann. Rev. Fluid Mech. **20**, 111–157 (1988)
12. Sierou, A., Brady, J.F.: Accelerated Stokesian dynamics simulations. J. Fluid Mech. **448**, 115–146 (2001)
13. Wang L., Li J.C., Zhou J.F.: An algorithm for coarse particle sedimentation simulation by Stokesian Dynamics. In: Proceeding of the 5th International Conference on Fluid Mechanics, pp. 432–435. Shanghai, China (2007)
14. Yan, Z.Y.: Theory of Low Reynolds Number Flow. Peking University Press, Beijing (2002) (in Chinese)
15. Durlofsky, L., Brady, J.F., Bossis, G.: Dynamic simulation of hydrodynamically interacting particles. J. Fluid Mech. **180**, 21–49 (1987)
16. Ichiki, K., Brady, J.F.: Many-body effects and matrix inversion in low-Reynolds-number hydrodynamics. Phys. Fluids **13**, 350–353 (2001)
17. Hasimoto, H.: On the periodic fundamental solutions of the Stokes equations and their application to viscous flow past a cubic array of sphere. J. Fluid Mech. **5**, 317–328 (1958)
18. Sangani, A.S., Acrivos, A.: Slow flow through a periodic array of spheres. Int. J. Multiphase Flow **8**, 343–360 (1982)
19. Zick, A.: Stokes flow through periodic arrays of spheres. J. Fluid Mech. **115**, 13–26 (1982)
20. Phillips, R.J., Brady, J.F., Bossis, G.: Hydrodynamic transport properties of hard-sphere dispersions. I. Suspensions of freely mobile particles. Phys. Fluids **31**, 3462–3472 (1988)
21. Ladd, A.J.C.: Hydrodynamic transport coefficients of random dispersions of hard spheres. J. Chem. Phys. **93**, 3484–3494 (1990)
22. Mo, G., Sangani, A.S.: A method for computing Stokes flow interactions among spherical objects and its application to suspensions of drops and porous particles. Phys. Fluids **6**, 1637–1652 (1994)